Room-Temperature Ferroelectric Resistive Switching in Ultrathin Pb(Zr$_{0.2}$Ti$_{0.8}$)O$_3$ Films

Daniel Pantel,* Silvana Goetze, Dietrich Hesse, and Marin Alexe

Max Planck Institute of Microstructure Physics, Weinberg 2, 06120 Halle (Saale), Germany

Due to their switchable spontaneous polarization, ferroelectric materials can be used as nonvolatile memories, *e.g.*, ferroelectric random access memories (FeRAM), but so far their destructive readout scheme limits the applications of ferroelectric memories.[1,2] Evaluating the polarization direction by a nondestructive readout scheme rather than by the switched charge would be a tremendous advantage. This has been recognized already from the early time of ferroelectric memories by development of the most simple nonvolatile memory cell: the ferroelectric field effect transistor (FeFET).[3,4] The major yet unsolved problem of FeFET is the low retention time, *i.e.*, the time within which the written information vanishes and the two polarization directions become indistinguishable. Losing information is most probably caused by the strongly asymmetric metal—ferroelectric—semiconductor structure, which generates polarization back-switching. Therefore, it will be highly desirable to find an alternative route to read nondestructively the polarization in a simple metal—ferroelectric—metal (MFM) structure, similar to the polar switch proposed by Esaki and co-workers.[5]

The leakage current in usual thin film ferroelectric capacitors is mostly governed by the band alignment at the metal—ferroelectric interface, the potential barrier, which itself is influenced by the polarization state.[6,7] Thus the effective resistance of a ferroelectric memory cell would have two bistable states like in resistive switching random access memories (RRAMs). In RRAMs these resistive effects are usually based on defects or on chemical processes[8,9] that may be difficult to control during the fabrication process.[10] On the contrary the resistive switching based on polarization switching in ferroelectrics is in principle a pure electronic process, and this might alleviate

ABSTRACT Spontaneous polarization of ferroelectric materials has been for a long time proposed as binary information support, but it suffers so far from destructive readout. A nondestructive resistive readout of the ferroelectric polarization state in a metal—ferroelectric—metal capacitor would thus be advantageous for data storage applications. Combing conducting force microscopy and piezoelectric force microscopy, we unambiguously show that ferroelectric polarization direction and resistance state are correlated for epitaxial ferroelectric Pb(Zr$_{0.2}$Ti$_{0.8}$)O$_3$ nanoscale capacitors prepared by self-assembly methods. For intermediate ferroelectric layer thickness (~9 nm) sandwiched between copper and La$_{0.7}$Sr$_{0.3}$MnO$_3$ electrodes we achieved giant electroresistance with a resistance ratio of >1500 and high switching current densities (>10 A/cm^2) necessary for effective resistive readout. The present approach uses metal—ferroelectric—metal devices at room temperature and, therefore, significantly advances the use of ferroelectric-based resistive switching.

KEYWORDS: ferroelectrics · resistive switching · nanoscale capacitor · conductive-AFM · PFM · Pb(Zr$_{0.2}$Ti$_{0.8}$)O$_3$

these drawbacks. Furthermore, ferroelectric polarization and thus the information stored in a memory cell can in principle be switched in the picosecond range,[11,12] as the effective switching time is usually limited only by the electrical circuit.[11,13]

Following this route, resistive switching in ferroelectrics has been intensively investigated in bulk crystals,[14] organic films,[15–17] and thin oxide films.[10,18–27] In this framework Maksymovych *et al.*,[21] using a conductive atomic force microscope (AFM) tip as a top electrode, showed that indeed the polarization direction influences Fowler—Nordheim tunneling into ferroelectrics. Nevertheless, for application in memory cells a real metal—ferroelectric—metal heterostructure, *i.e.*, a capacitor, is required. The capacitor geometry would exclude any spurious effects on the resistance due, for instance, to electrochemical interaction between the AFM tip and the ferroelectric surface.[28–30] Furthermore, the uniform electric field in the case of a capacitor-like geometry provides better physical insight into the switching and transport mechanism.[31]
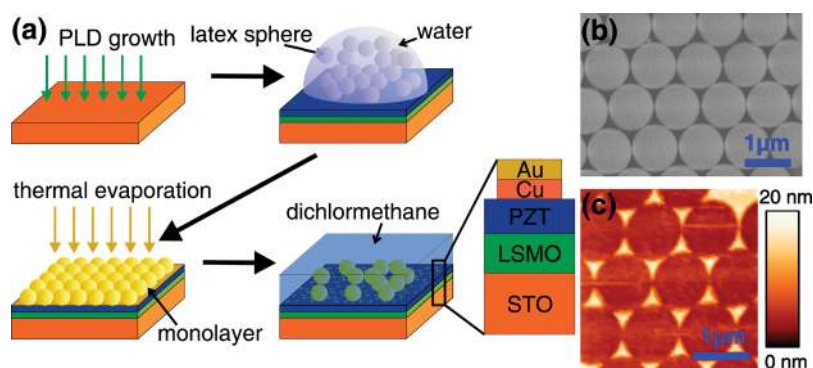
Figure 1. (a) Schematic of the NSL process adapted for nanoscale electrode preparation on PZT surfaces. (b) Scanning electron microscopy (SEM) image of a hexagonally close packed monolayer of polysterene spheres and (c) the resulting Au-capped Cu nanoislands (by AFM) on top of a PZT surface.

Electroresistance effects have been found in ferroelectric thin films with real metal electrodes,[10,24,26,27] but it is not yet unambiguously shown that these effects are solely based on the ferroelectric switching.

Here, we apply a self-assembly approach to prepare large arrays of well-ordered ferroelectric capacitors with typical sizes smaller than 0.1 μm^2. We clearly show the direct correlation between polarization switching and resistive switching in MFM heterostructures with ultrathin epitaxial ferroelectric lead zirconate titanate, $Pb(Zr_{0.2}Ti_{0.8})O_3$ (PZT), films by measuring the current through a gold-capped $Cu/PZT/La_{0.7}Sr_{0.3}MnO_3$ (LSMO) capacitor with a *ca.* 9 nm thick ferroelectric PZT layer and the polarization direction using conducting force microscopy (C-AFM) and piezoelectric force microscopy (PFM), respectively.

Ferroelectric PZT was chosen as a model room-temperature ferroelectric material that can be epitaxially grown, almost defect free, on $SrTiO_3$ (STO) substrates, giving a high spontaneous polarization,[32] and can even be integrated onto silicon.[33] Usual ferroelectric capacitors have a typical electrode area on the order of several tens or hundreds of square micrometers, and usually the defect-mediated leakage paths will rule the overall current and obscure the polarization-dependent current for ultrathin ferroelectric films. In order to avoid this, submicrometer capacitors have to be used.

We use natural lithography[34] or nanosphere lithography (NSL)[35,36] to fabricate arrays of well-ordered nanoscale ferroelectric capacitors. NSL is a versatile lithography technique producing well-ordered masks with scalable pitch and feature size relying on the self-assembly of a mono or double layer of hexagonally close-packed polystyrene latex spheres.[34−36] First it was applied to produce ordered arrays of metal nanoislands, but later on also to the growth of ordered 1D nanostructures,[37] ferroelectric nanodots,[38] magnetic nanodots,[39] and organic semiconductor particles.[35] Here, we use nanosphere lithography to produce arrays of well-ordered metal electrodes on the top ferroelectric surface.

RESULTS AND DISCUSSION

The MFM preparation process is sketched in Figure 1a. First, the oxide layers were grown by pulsed laser deposition (PLD) at elevated temperature. Directly after cooling, the samples were removed from the PLD chamber and NSL was applied. Details of the NSL process can be found in the Methods section. The self-assembled monolayer of polystyrene latex spheres (1 μm diameter) was subsequently used as a stencil mask for thermal evaporation of the metal layers (here Cu capped with Au). Figure 1b shows the perfect self-assembly of the spheres into a monolayer on the PZT surface after metal deposition. Copper was chosen as the top electrode since it gives good Schottky barriers with PZT.[40] The resulting well-ordered metal nanostructures (Figure 1c) were obtained by dissolving the latex nanospheres in dichloromethane.

Transport and piezoelectric measurements are then performed by contacting the nanoscale top electrode using an AFM tip (schematically sketched in the inset of Figure 3) through which *IV* curves (C-AFM mode) and piezoelectric characteristics (PFM) are measured.

For the present Cu/PZT/LSMO heterostructures, two issues in terms of film quality need to be addressed to unambiguously analyze measured transport data through ultrathin ferroelectric films. First, the LSMO bottom electrode needs to be almost perfect in terms of the structural quality and surface morphology. An atomically flat surface is necessary to avoid any current inhomogeneity. Second, one needs to have an effective resistance much smaller than the junction resistance to avoid current limiting by a parasitic serial resistance. Thus the actual resistivity needs to be as low as possible, and a high enough LSMO thickness to ensure a low effective resistance is necessary. The optimum thickness of the LSMO bottom electrode was found to be around 50 nm with its typical properties being shown in the Supporting Information.

Another important issue is the PZT polarization, since the electroresistance scales exponentially with polarization value.[41] It is known that polarization
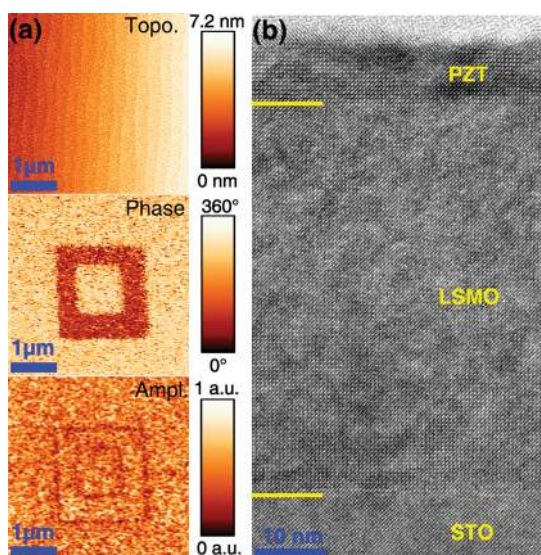
Figure 2. (a) Topographic and piezoresponse AFM images of a *ca.* 9 nm thick epitaxial PZT film after poling two squares in an as-grown region with a voltage of $-2\,V$ ($2 \times 2\,\mu m^2$) and $+2\,V$ ($1 \times 1\,\mu m^2$) applied between bottom electrode and the conductive AFM tip. A PFM-phase change by $180°$ with no observable topographic change confirms the ferroelectric nature of the PZT film. (b) HR-TEM micrograph of the same PZT/LSMO/STO heterostructure.

Figure 3. (a) Current density *j versus* voltage *V* on a 1.5 μm^2 and a 0.04 μm^2 Cu/Au island on a *ca.* 9 nm thick PZT film measured by different conductive coating of AFM tips (Ti−Pt and conductive diamond, respectively) as sketched in the inset, demonstrating that electrode size and tip do not influence the result. (b) Electroresistance ER and ON/ OFF ratio *versus* operation voltage *V* calculated for the 1.5 μm^2 device from (a). All lines are guides to the eye.

decreases as the film thickness decreases below 10 nm.[42−45] We have shown that a very high electroresistance is given by the thermionic injection (Schottky) transport mechanism or by changing the transport mechanism from thermionic injection to Fowler−Nordheim tunneling by polarization direction.[31] The thickness range where this is suitable in terms of low voltage and sufficiently high current density is rather narrow. For PZT the optimum thickness will be approximately in the range of 4 to 10 nm. Indeed, for a 20 nm thick PZT film almost no current can be measured for voltages below coercive voltage.

For the present case the ferroelectricity was confirmed by PFM for the films thinner than 10 nm. Figure 2a shows poling experiments on a bare PZT surface for the primarily investigated 9 nm thick PZT film. In the as-grown state the polarization points upward, *i.e.*, toward the AFM tip, like in the case of a positively poled surface. The poled ferroelectric domain configuration is stable for at least several hours. Thicker PZT films (20 nm or more) grown at the same conditions show on macroscopic capacitors (0.04 mm²) fully saturated ferroelectric polarization loops with a high remnant polarization of about 110 $\mu C/cm^2$ (Supporting Information), confirming the excellent ferroelectric properties of our PZT films.[32] The high remnant polarization is in agreement with the large out-of-plane lattice constant resulting from the in-plane compressive stress from the STO substrate of the PZT layers, as shown by X-ray investigations. All our heterostructures are grown fully strained to the STO lattice, as confirmed by reciprocal space mappings around the STO 203
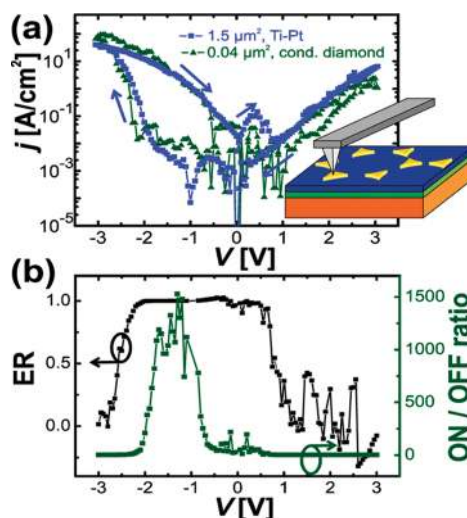
reflection (Supporting Information), ensuring high polarization even for ultrathin films. High-resolution transmission electron microscope images (Figure 2b) indicate coherent growth with sharp interfaces.

Figure 3a shows *IV* characteristics of a 1.5 μm^2 and a 0.04 μm^2 Au-capped Cu electrode on top of a 9 nm thick PZT film. A large hysteresis in current is observed for both devices. It is worth noting that devices with a large difference in area show similar current densities (see also Figure S4 in Supporting Information), which is a strong indication for a homogeneous transport over the electrode area, in contrast to a filament- or defect-controlled transport. By running from $+3\,V$ to $-3\,V$, the current switches from the low conducting state (OFF) to the high conducting state (ON) at approximately $-2.1\,V$ and back to the OFF state at about 0.8 V when sweeping from -3 V to $+3$ V, as the polarization presumably switches. The switching voltage varies slightly from device to device. The OFF state is for the polarization up and the ON state is for polarization down, with the as-grown state being OFF, in agreement with the as-grown upward polarization direction deduced from Figure 2a. The displacement current peaks, clearly visible in Figure S3a, cannot be seen here because of the long measurement time as well as the low expected current density compared to the current density in the ON state. The switching behavior is observed for most of the investigated devices, although some show high, not switchable leakage, probably because of conducting paths due to clustering of defects underneath those electrodes.
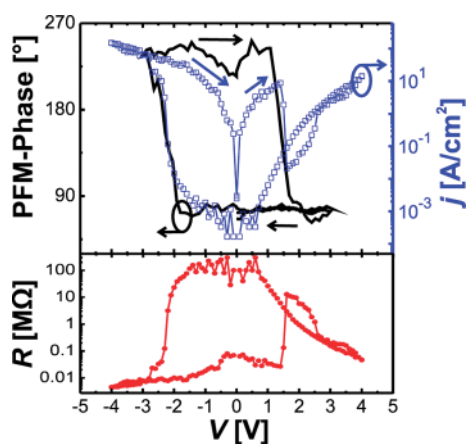
Figure 4. *IV* and remnant PFM-phase hysteresis on the same device (thickness: 9 nm, area: 0.6 μm^2) in consecutive measurements. The coercive voltages of ferroelectric switching and current switching are identical within the limits of the ac PFM probing voltage of 0.5 V. The lower panel provides additionally the voltage, *V*, dependence of the resistance, *R*.

The electroresistance (ER) is given by

$$ER = \frac{j(P^{\downarrow}, ON) - j(P^{\uparrow}, OFF)}{j(P^{\downarrow}, ON)} \qquad (1)$$

where *j* is the current density, which approaches in our case unity; that is, the ratio between ON and OFF states exceeds about 100, at reasonable operation voltages below the switching voltage (see Figure 3b). However, the ON/OFF ratio rises to 1500 (at −1.3 V), being higher than in C-AFM based reports,[23,20,22] as expected by the thickness dependence of the electroresistance.[31,23] The switched current density exceeds 10 A/cm^2 at voltages below the switching voltage, higher than in Pt/BiFeO$_3$/SrRuO$_3$ heterostructures with much thicker ferroelectric layers.[10]

To establish a direct correlation between ferroelectric and resistive switching, simultaneous or consecutive measurements of the voltage dependence of a ferroelectric parameter, *e.g.*, polarization, and the current on the same device are necessary.[19,21] Here, we consecutively measure the *IV* characteristics and then the piezoelectric loop on the same capacitor (Figure 4). The *IV* characteristics show switching voltages of approximately 1.4 and −2.2 V. As expected, for ferroelectric polarization switching, the PFM phase changes by 180° at the coercive voltages (1.4 and −2.2 V, corresponding to a coercive field of about 2 MV/cm, on the order of what is observed in ultrathin ferroelectric films[21−23]); that is, the coercive voltage and the voltage at which the resistance switches coincide. Therefore we conclude that the resistive switching is originating in ferroelectric switching. Due to the small size of the electrodes and the low currents, heating effects of the tip are negligible.[19] Hence, we do not see that the current influences the piezoelectric measurements.
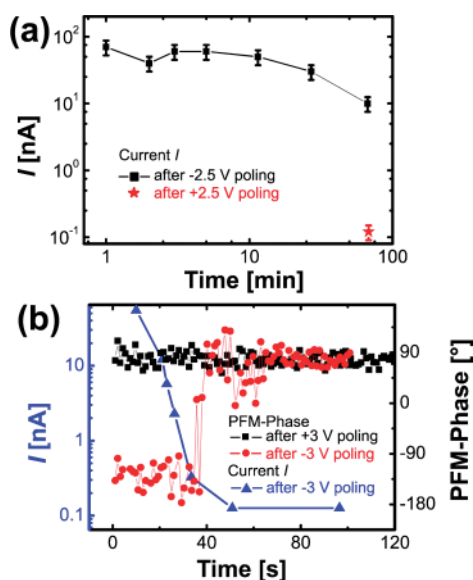

Figure 5. (a) Retention properties of a typical capacitor after switching with −2.5 V recorded at −1.7 V, demonstrating a long retention time. The error bars indicate the current fluctuations during the measurement. Other capacitors have smaller retention times, as shown in (b). The time dependency of the PFM phase after switching with ±3 V and the current state at −1 V after switching with −3 V show that back-switching of the polarization from down to up occurs on the same time scale as the transition from high to low conduction state. All lines are guides to the eye.

Retention is an important issue for the nonvolatile memory cells, which in the case of ferroelectric memories is due to polarization back-switching or imprint phenomena.[2] In the present case retention provides additional evidence for the ferroelectric origin of the resistive switching. Some electrodes show stable current states of the negatively poled state (ON state, polarization down) for more than one hour (Figure 5a). However, few devices (see Figure 5b) show rapid back-switching of the polarization from down to up as observed in the PFM-phase signal by a change of 180° after several 10 seconds. As shown in Figure 5b, the current density of the same electrodes decays on a similar time scale, which is in agreement with a polarization back-switching scenario. This observation excludes any voltage-driven electrochemical effects on the resistive switching, since during polarization and resistive back-switching there is no electrical field applied. The rather broad transition in current compared to the switching in PFM phase is mostly due to the difference in the effect of polarization switching on the mechanical behavior (vibrations by piezoelectric effect) and the electronic conduction: The polarization switching proceeds by nucleation and growth even for nanoscale capacitors,[46] which means that at certain stages during the back-switching the capacitor will consist of domains with different orientations. While the phase switches by 180° when more than 50% of the area is switched, the influence of the polarization

on the current is exponential and may lead to an earlier change in current during polarization back-switching.

One of the most important questions is related to the transport mechanism that governs the electroresistance. As the ferroelectric films are relatively thick (9 nm), direct tunneling is rather unlikely. For the investigated ferroelectric barrier thickness thermionic injection is expected to prevail on the electronic transport at room temperature.[31] The corresponding electric field (E) dependency of the current density ($j_{Schottky}$) for simple semiconductors is given by[47]

$$j_{Schottky} = A^{**}T^2 \exp\left[-\frac{1}{k_B T}\left(\Phi_B - \sqrt{\frac{e^3 E}{4\pi\varepsilon_0\varepsilon_{ifl}}}\right)\right] \tag{2}$$

with temperature T, the effective Richardson's constant A^{**}, the image force lowering permittivity ε_{ifl}, and the potential barrier Φ_B. The electric field E for a ferroelectric material is a superposition of the applied field, the depolarization field, and the field due to the band alignment.[7] In the Supporting Information (Figure S5), we show a fit of the obtained IV data to eq 2, from which we conclude that indeed thermionic injection dominates the transport for the investigated film. The obtained changes in barrier heights from 0.57 and 0.67 eV in the ON state to 1.33 and 0.63 eV in the OFF state are consistent with the electrostatic model for the dependence of an asymmetric barrier on the polarization direction of a metal–ferroelectric–metal heterostructure.[41]

Higher currents necessary for the use of low-cost current amplifiers in memory applications[9,10] can be achieved in high-quality ferroelectric films with thicknesses below about 4 nm by tunneling,[31] which also provides electroresistance,[48,41,20] or by using semiconductor ferroelectrics.[10]

CONCLUSIONS

In summary, we have shown an approach to prepare nanoscale metal–ferroelectric–metal capacitors using self-assembly methods. These nanoscale capacitors are subsequently used to clearly show the direct correlation between resistive and ferroelectric switching in ultrathin PZT films. A high resistance ratio, up to 1500, as well as high switched current densities of about 10 A/cm^2 open new pathways toward ferroelectricity-based nonvolatile memory devices.

METHODS

Sample Preparation. PLD was performed at substrate temperatures between 550 and 600 °C in an oxygen atmosphere of 0.2 mbar ablating stoichiometric ceramic targets (with 10% Pb excess for the PZT target). Base pressure of our PLD system is below 5×10^{-6} mbar. The energy fluence of the KrF excimer laser ($\lambda = 248$ nm) at the target was about 300 mJ/cm^2. The 0.1° off-cut STO (100)-oriented substrates were etched and annealed before deposition to obtain an atomically flat, single TiO$_2$-terminated surface with approximately 200 nm wide terraces separated by one unit cell high steps.[49]

For NSL a commercial water solution of monodisperse polysterene latex spheres (2.5 wt %) was diluted 1:1 by volume with isopropyl alcohol (*p.a.*) to reduce surface tension. For the 1 μm diameter spheres, 5 μL of the obtained solution was dripped on the approximately 10° tilted sample surface and dried at room temperature. More details on NSL can be found in the Supporting Information.

For thermal evaporation, the Cu and Au were evaporated from a tungsten coil and boat, respectively, at a distance of 10 cm from the sample. The sample could be moved to allow for metal heterostructures with the thicknesses controlled by a quartz crystal. The pressure during the room-temperature deposition process was kept below 7×10^{-6} mbar to prevent oxidation.

Piezoelectric Force and Conductive Scanning Probe Microscopy. The AFM-based investigations were carried out using a CP-Research microscope (Thermomicroscope) with a variety of conductive AFM tips (ATEC-EFM/Ir–Pt, NSC15/Ti–Pt, DDESP-FM/doped diamond, CDT-FMR/doped diamond) in contact mode. A lock-in amplifier (SR 830 DSP) was used to apply the ac probing voltage ($f = 24.5$ kHz) with an amplitude of 0.5 V, well below the coercive voltage of the PZT films, to the bottom electrode and to measure the piezoresponse signal. Direct current voltage pulses were also superimposed for remnant hysteresis measurements by the lock-in amplifier, where the piezoresponse was measured at $V_{dc} = 0$ V after poling with an applied voltage for 200 ms.

For collecting IV curves the measured current was amplified by 10^8 V/A with a variable gain sub femto ampere current amplifier (Femto DDCPA-300) and subsequently by ×10 (low-noise preamplifier, SR 560) and filtered with a low pass filter (1 kHz). The resulting voltage, proportional to the current, was measured by a Keithley Multimeter 2000. The IV measurement setup was previously calibrated using a Keithley Electrometer 6517B connected to the tip. A 1 MΩ serial resistor limited the current through the AFM tip. A full voltage sweep took about 10 s, *i.e.*, on the same time scale as the PFM loops.

For the retention measurement the polarization was switched by a voltage pulse (-3 V, 1 s) into a defined polarization state. Consecutively, the voltage was held at 0 V. To measure the current after a certain retention time, the voltage was set to -1 V, and after 1 s (to let the current relax into a stable state) the current was measured.

Transmission Electron Microscopy. High-resolution TEM investigations were performed using a Jeol 4010 microscope. TEM samples were prepared by standard methods (mechanical polishing and ion milling).

Supporting Information Available: Details for NSL, LSMO properties, PZT properties, additional electrical measurements on nanoscale capacitors, and fits of the IV curves to the thermionic injection model. This material is available free of charge *via* the Internet at http://pubs.acs.org.

REFERENCES AND NOTES

1. Auciello, O.; Scott, J. F.; Ramesh, R. The Physics of Ferroelectric Memories. *Phys. Today* **1998**, *51*, 22–27.
2. Scott, J. *Ferroelectric Memories*; Springer: Berlin, 2000.

3. Looney, D. H.; Summit, N. J. *Semiconductive Translating Device*. US Patent 2,791,758, 1957.

4. Wu, S.-Y.; Francombe, M. H. *Ferroelectric Memory Device*. US Patent 3,832,700, 1974.

5. Esaki, L.; Laibowitz, R.; Stiles, P. Polar Switch. *IBM Tech. Disclosure Bull.* **1971**, *13*, 2161.

6. Chang, L.; Esaki, L. Nonvolatile Schottky Diode with Barrier Height Controlled by Ferroelectric Polarization. *IBM Tech. Disclosure Bull.* **1971**, *14*, 1250–1251.

7. Pintilie, L.; Vrejoiu, I.; Hesse, D.; LeRhun, G.; Alexe, M. Ferroelectric Polarization-Leakage Current Relation in High Quality Epitaxial $Pb(Zr,Ti)O_3$ Films. *Phys. Rev. B* **2007** *75*, 104103.

8. Waser, R.; Aono, M. Nanoionics-Based Resistive Switching Memories. *Nat. Mater.* **2007**, *6*, 833–840.

9. Waser, R.; Dittmann, R.; Staikov, G.; Szot, K. Redox-Based Resistive Switching Memories - Nanoionic Mechanisms, Prospects, and Challenges. *Adv. Mater.* **2009**, *21*, 2632.

10. Jiang, A. Q.; Wang, C.; Jin, K. J.; Liu, X. B.; Scott, J. F.; Hwang, C. S.; Tang, T. A.; Liu, H. B.; Yang, G. Z. A Resistive Memory in Semiconducting $BiFeO_3$ Thin-Film Capacitors. *Adv. Mater.* **2011**, *23*, 1277–1281.

11. Li, J.; Nagaraj, B.; Liang, H.; Cao, W.; Lee, C. H.; Ramesh, R. Ultrafast Polarization Switching in Thin-Film Ferroelectrics. *Appl. Phys. Lett.* **2004**, *84*, 1174–1176.

12. Korff Schmising, C. v.; Bargheer, M.; Kiel, M.; Zhavoronkov, N.; Woerner, M.; Elsaesser, T.; Vrejoiu, I.; Hesse, D.; Alexe, M. Coupled Ultrafast Lattice and Polarization Dynamics in Ferroelectric Nanolayers. *Phys. Rev. Lett.* **2007**, *98*, 257601.

13. Jiang, A. Q.; Lin, Y. Y.; Tang, T. A. Interfacial-Layer Modulation of Domain Switching Current in Ferroelectric Thin Films. *J. Appl. Phys.* **2007**, *101*, 104105.

14. Choi, T.; Lee, S.; Choi, Y. J.; Kiryukhin, V.; Cheong, S.-W. Switchable Ferroelectric Diode and Photovoltaic Effect in $BiFeO_3$. *Science* **2009**, *324*, 63–66.

15. Qu, H.; Yao, W.; Garcia, T.; Zhang, J.; Sorokin, A. V.; Ducharme, S.; Dowben, P. A.; Fridkin, V. M. Nanoscale Polarization Manipulation and Conductance Switching in Ultrathin Films of a Ferroelectric Copolymer. *Appl. Phys. Lett.* **2003**, *82*, 4322–4324.

16. Asadi, K.; de Leeuw, D. M.; de Boer, B.; Blom, P. W. M. Organic Non-Volatile Memories from Ferroelectric Phase-Separated Blends. *Nat. Mater.* **2008**, *7*, 547–550.

17. López-Encarnación, J. M.; Burton, J. D.; Tsymbal, E. Y.; Velev, J. P. Organic Multiferroic Tunnel Junctions with Ferroelectric Poly(vinylidene fluoride) Barriers. *Nano Lett.* **2011**, *11*, 599–603.

18. Shen, W.; Dittmann, R.; Breuer, U.; Waser, R. Improved Endurance Behavior of Resistive Switching in $(Ba,Sr)TiO_3$ Thin Films with W Top Electrode. *Appl. Phys. Lett.* **2008**, *93*, 222102–3.

19. Kohlstedt, H.; Petraru, A.; Szot, K.; Rudiger, A.; Meuffels, P.; Haselier, H.; Waser, R.; Nagarajan, V. Method to Distinguish Ferroelectric from Nonferroelectric Origin in Case of Resistive Switching in Ferroelectric Capacitors. *Appl. Phys. Lett.* **2008**, *92*, 062907.

20. Garcia, V.; Fusil, S.; Bouzehouane, K.; Enouz-Vedrenne, S.; Mathur, N. D.; Barthelemy, A.; Bibes, M. Giant Tunnel Electroresistance for Non-Destructive Readout of Ferroelectric States. *Nature* **2009**, *460*, 81–84.

21. Maksymovych, P.; Jesse, S.; Yu, P.; Ramesh, R.; Baddorf, A. P.; Kalinin, S. V. Polarization Control of Electron Tunneling into Ferroelectric Surfaces. *Science* **2009**, *324*, 1421–1425.

22. Crassous, A.; Garcia, V.; Bouzehouane, K.; Fusil, S.; Vlooswijk, A. H. G.; Rispens, G.; Noheda, B.; Bibes, M.; Barthelemy, A. Giant Tunnel Electroresistance with $PbTiO_3$ Ferroelectric Tunnel Barriers. *Appl. Phys. Lett.* **2010**, *96*, 042901.

23. Gruverman, A.; Wu, D.; Lu, H.; Wang, Y.; Jang, H. W.; Folkman, C. M.; Zhuravlev, M. Y.; Felker, D.; Rzchowski, M.; Eom, C. B.; *et al.* Tunneling Electroresistance Effect in Ferroelectric Tunnel Junctions at the Nanoscale. *Nano Lett.* **2009**, *9*, 3539–3543.

24. Blom, P. W. M.; Wolf, R. M.; Cillessen, J. F. M.; Krijn, M. P. C. M. Ferroelectric Schottky Diode. *Phys. Rev. Lett.* **1994**, *73*, 2107–2110.

25. Yang, C.-H.; Seidel, J.; Kim, S. Y.; Rossen, P. B.; Yu, P.; Gajek, M.; Chu, Y. H.; Martin, L. W.; Holcomb, M. B.; He, Q.; *et al.* Electric Modulation of Conduction in Multiferroic Ca-doped $BiFeO_3$ Films. *Nat. Mater.* **2009**, *8*, 485–493.

26. Garcia, V.; Bibes, M.; Bocher, L.; Valencia, S.; Kronast, F.; Crassous, A.; Moya, X.; Enouz-Vedrenne, S.; Gloter, A.; Imhoff, D.; *et al.* Ferroelectric Control of Spin Polarization. *Science* **2010**, *327*, 1106.

27. Hambe, M.; Petraru, A.; Pertsev, N. A.; Munroe, P.; Nagarajan, V.; Kohlstedt, H. Crossing an Interface: Ferroelectric Control of Tunnel Currents in Magnetic Complex Oxide Heterostructures. *Adv. Funct. Mater.* **2010**, *20*, 2436–2441.

28. Dagata, J. A.; Schneir, J.; Harary, H. H.; Evans, C. J.; Postek, M. T.; Bennett, J. Modification of Hydrogen-Passivated Silicon by a Scanning Tunneling Microscope Operating in Air. *Appl. Phys. Lett.* **1990**, *56*, 2001–2003.

29. Kalinin, S. V.; Morozovska, A. N.; Chen, L. Q.; Rodriguez, B. J. Local Polarization Dynamics in Ferroelectric Materials. *Rep. Prog. Phys.* **2010**, *73*, 056502.

30. Kalinin, S. V.; Balke, N. Local Electrochemical Functionality in Energy Storage Materials and Devices by Scanning Probe Microscopies: Status and Perspectives. *Adv. Mater.* **2010**, *22*, E193–E209.

31. Pantel, D.; Alexe, M. Electroresistance Effects in Ferroelectric Tunnel Barriers. *Phys. Rev. B* **2010**, *82*, 134105.

32. Vrejoiu, I.; Le Rhun, G.; Pintilie, L.; Hesse, D.; Alexe, M.; Goesele, U. Intrinsic Ferroelectric Properties of Strained Tetragonal $PbZr_{0.2}Ti_{0.8}O_3$ Obtained on Layer by Layer Grown, Defect Free Single Crystalline Films. *Adv. Mater.* **2006**, *18*, 1657–1661.

33. Sambri, A.; Gariglio, S.; Pardo, A. T.; Triscone, J.-M.; Stéphan, O.; Reiner, J. W.; Ahn, C. H. Enhanced Critical Temperature in Epitaxial Ferroelectric $Pb(Zr_{0.2}Ti_{0.8})O_3$ Thin Films on Silicon. *Appl. Phys. Lett.* **2011**, *98*, 012903.

34. Deckman, H.; Dunsmuir, J. Natural Lithography. *Appl. Phys. Lett.* **1982**, *41*, 377–379.

35. Hulteen, J. C.; Van Duyne, R. P. Nanosphere Lithography - A Materials General Fabrication Process for Periodic Particle Array Surfaces. *J. Vac. Sci. Technol. A* **1995**, *13*, 1553–1558.

36. Hulteen, J. C.; Treichel, D. A.; Smith, M. T.; Duval, M. L.; Jensen, T. R.; Van Duyne, R. P. Nanosphere lithography: Size-Tunable Silver Nanoparticle and Surface Cluster Arrays. *J. Phys. Chem. B* **1999**, *103*, 3854–3863.

37. Li, L.; Zhai, T.; Zeng, H.; Fang, X.; Bando, Y.; Golberg, D. Polystyrene Sphere-Assisted One-Dimensional Nanostructure Arrays: Synthesis and Applications. *J. Mater. Chem.* **2011**, *21*, 40–56.

38. Ma, W.; Harnagea, C.; Hesse, D.; Goesele, U. Well-Ordered Arrays of Pyramid-Shaped Ferroelectric $BaTiO_3$ Nanostructures. *Appl. Phys. Lett.* **2003**, *83*, 3770–3772.

39. Winzer, M.; Kleiber, M.; Dix, N.; Wiesendanger, R. Fabrication of Nanodot- and Nanoring-arrays by Nanosphere Lithography. *Appl. Phys. A: Mater. Sci. Process* **1996**, *63*, 617–619.

40. Pintilie, L.; Vrejoiu, I.; Hesse, D.; Alexe, M. The Influence of the Top-Contact Metal on the Ferroelectric Properties of Epitaxial Ferroelectric $Pb(Zr_{0.2}Ti_{0.8})O_3$ Thin Films. *J. Appl. Phys.* **2008**, *104*, 114101.

41. Zhuravlev, M. Y.; Sabirianov, R. F.; Jaswal, S. S.; Tsymbal, E. Y. Giant Electroresistance in Ferroelectric Tunnel Junctions. *Phys. Rev. Lett.* **2005**, *94*, 246802.

42. Junquera, J.; Ghosez, P. Critical Thickness for Ferroelectricity in Perovskite Ultrathin Films. *Nature* **2003**, *422*, 506–509.

43. Kim, Y. S.; Kim, D. H.; Kim, J. D.; Chang, Y. J.; Noh, T. W.; Kong, J. H.; Char, K.; Park, Y. D.; Bu, S. D.; Yoon, J.-G.; *et al*. Critical Thickness of Ultrathin Ferroelectric $BaTiO_3$ Films. *Appl. Phys. Lett.* **2005**, *86*, 102907.

44. Nagarajan, V.; Junquera, J.; He, J. Q.; Jia, C. L.; Waser, R.; Lee, K.; Kim, Y. K.; Baik, S.; Zhao, T.; Ramesh, R.; *et al*. Scaling of Structure and Electrical Properties in Ultrathin Epitaxial Ferroelectric Heterostructures. *J. Appl. Phys.* **2006**, *100*, 051609.

45. Petraru, A.; Kohlstedt, H.; Poppe, U.; Waser, R.; Solbach, A.; Klemradt, U.; Schubert, J.; Zander, W.; Pertsev, N. A.

Wedgelike Ultrathin Epitaxial BaTiO$_3$ Films for Studies of Scaling Effects in Ferroelectrics. *Appl. Phys. Lett.* **2008**, *93*, 072902.

46. Kim, Y.; Han, H.; Lee, W.; Baik, S.; Hesse, D.; Alexe, M. Non-Kolmogorov-Avrami-Ishibashi Switching Dynamics in Nanoscale Ferroelectric Capacitors. *Nano Lett.* **2010**, *10*, 1266–1270.

47. Sze, S. *Physics of Semiconductor Devices*; Wiley-Interscience: Hoboken, NJ, 2007.

48. Kohlstedt, H.; Pertsev, N. A.; Rodriguez Contreras, J.; Waser, R. Theoretical Current-Voltage Characteristics of Ferroelectric Tunnel Junctions. *Phys. Rev. B* **2005**, *72*, 125341.

49. Koster, G.; Kropman, B. L.; Rijnders, G. J. H. M.; Blank, D. H. A.; Rogalla, H. Quasi-Ideal Strontium Titanate Crystal Surfaces Through Formation of Strontium Hydroxide. *Appl. Phys. Lett.* **1998**, *73*, 2920–2922.

Correction to Room-Temperature Ferroelectric Resistive Switching in Ultrathin Pb(Zr$_{0.2}$Ti$_{0.8}$)O$_3$ Films [*ACS Nano* **2011,** *5*, 6032–6038. DOI: 10.1021/nn2018528].

Daniel Pantel,* Silvana Goetze, Dietrich Hesse, and Marin Alexe

In the lower part of Figure 4, the resistance *R* should be given in units of GΩ instead of MΩ. This does not influence any conclusions drawn from the article.
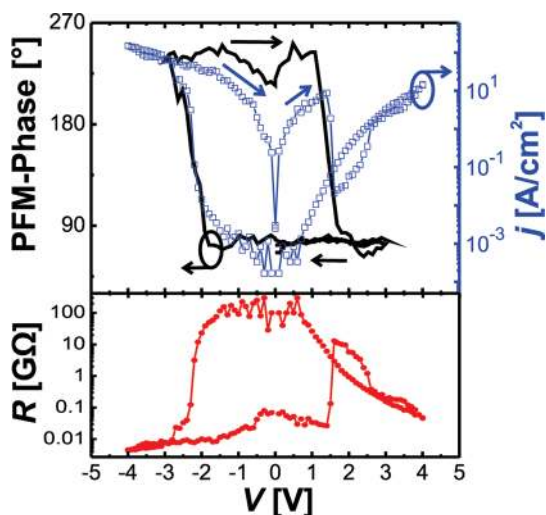

Figure 4. *IV* and remnant PFM-phase hysteresis on the same device (thickness: 9 nm, area: 0.6 μm^2) in consecutive measurements. The coercive voltages of ferroelectric switching and current switching are identical within the limits of the ac PFM probing voltage of 0.5 V. The lower panel provides additionally the voltage, *V*, dependence of the resistance, *R*.